Available online at www.sciencedirect.com
ScienceDirect
International Journal of Heat and Mass Transfer 51 (2008) 2733–2741
International Journal of HEAT and MASS TRANSFER
www.elsevier.com/locate/ijhmt

Finite element simulations of natural convection flow in an isosceles triangular enclosure filled with a porous medium: Effects of various thermal boundary conditions

Tanmay Basak [a], S. Roy [b], S. Krishna Babu [b], I. Pop [c,*]

[a] Department of Chemical Engineering, Indian Institute of Technology Madras, Chennai 600 036, India
[b] Department of Mathematics, Indian Institute of Technology Madras, Chennai 600 036, India
[c] Faculty of Mathematics, University of Cluj, R-3400 Cluj, CP 253, Romania

Received 3 April 2007
Available online 21 February 2008

Abstract

The phenomena of natural convection in an isosceles triangular enclosure filled with a porous matrix has been studied numerically. A penalty finite element analysis with bi-quadratic elements is used for solving the Navier–Stokes and energy balance equations. The detailed study is carried out in two cases depending on various thermal boundary conditions; case I: two inclined walls are uniformly heated while the bottom wall is isothermally cooled and case II: two inclined walls are non-uniformly heated while the bottom wall is isothermally cooled. The present numerical procedure adopted in this investigation yields consistent performance over a wide range of parameters, Darcy number, Da ($10^{-5} \leqslant Da \leqslant 10^{-3}$), Rayleigh number, Ra ($10^3 \leqslant Ra \leqslant 10^6$) and Prandtl number, Pr ($0.026 \leqslant Pr \leqslant 10$) for all the cases mentioned above. Numerical results are presented in terms of stream functions, temperature profiles and Nusselt numbers. It has been found that at low Darcy numbers ($Da \leqslant 10^{-5}$) the heat transfer is primarily due to conduction irrespective of the Ra and Pr. In this regime, the isotherms are almost parallel near the bottom portion of the triangular enclosure whereas at $Da = 10^{-3}$, the isotherms are more distorted. As Rayleigh number increases, there is a change from conduction dominant region to convection dominant region for $Da = 10^{-3}$, and the critical Rayleigh number corresponding to on-set of convection is obtained. Some interesting features of stream function and isotherm contours are discussed especially for low and high Prandtl number limits. Complete heat transfer analysis is performed in terms of local and average Nusselt numbers.

Keywords: Natural convection; Triangular enclosure; Porous matrix; Linear heating; Critical Rayleigh number; Penalty finite element method

1. Introduction

The phenomena of convective motion of fluid, a well-known buoyancy driven phenomena, has attracted many researchers over the past few years. In this context, non-Darcy effects on natural convection in porous media have received a great deal of attention. This is due to large number of applications, such as, oil extraction, fluid flow in geothermal reservoirs, solid matrix heat exchangers, iron blast furnaces, energy efficient drying processes, ground water hydrology, solidification of casting etc. In recent years, triangular enclosures have received a considerable attention because of their applicability in various fields such as, building and thermal insulation systems, solar engineering applications, etc.

A good amount of literature is available on the convection patterns in enclosures filled with porous media (see [1–4]). The buoyancy driven convection in a differentially heated porous cavity has been analyzed by Walker and Homsy [5] with various techniques which yield a complete description of two-dimensional solutions. The Brinkman-extended Darcy model has been studied by Tong and Subr-

* Corresponding author.
E-mail addresses: tanmay@iitm.ac.in (T. Basak), sjroy@iitm.ac.in (S. Roy), pop.ioan@yahoo.co.uk (I. Pop).

0017-9310/$ - see front matter © 2007 Elsevier Ltd. All rights reserved.
doi:10.1016/j.ijheatmasstransfer.2007.10.009

Nomenclature

Da	Darcy number
g	acceleration due to gravity, m s^{-2}
k	thermal conductivity, W m^{-1} K^{-1}
K	permeability of the porous medium
L	height of the triangular cavity, m
Nu	Nusselt number
p	pressure, Pa
P	dimensionless pressure
Pr	Prandtl number
Ra	Rayleigh number
T	temperature, K
T_h	temperature of hot inclined wall, K
T_c	temperature of cold bottom wall, K
u, v	x and y components of dimensional velocities, ms^{-1}, respectively
U, V	x and y components of dimensionless velocities respectively
X, Y	dimensionless distances along x and y coordinates, respectively

Greek symbols

α	thermal diffusivity, m^2 s^{-1}
β	volume expansion coefficient, K^{-1}
γ	penalty parameter
ξ, η	horizontal and vertical coordinates in a unit square, respectively
ν	kinematic viscosity, m^2 s^{-1}
θ	dimensionless temperature
ρ	density, kg m^{-3}
Φ	basis functions
ψ	stream function

Subscripts

b	bottom wall
l	left wall
r	right wall
s	side wall

amanian [6], and Lauriat and Prasad [7] to investigate the buoyancy effects on natural convection in a vertical cavity. However, this model does not provide adequate analysis for the transition from porous medium flow to pure fluid flow as the permeability is more in the case of porous medium. A model that bridges the gap between the Darcy and Navier–Stokes equations is the Darcy–Forchheimer model developed by Vafai and Tien [8]. In addition, this model describes the effects of inertia and viscous forces in porous media and was used by Poulikakos and Bejan [9], Poulikakos [10], Lauriat and Prasad [11] to investigate the free convection in a vertical porous layer and in a vertical enclosure filled with a porous medium. Very recently Basak et al. [12] studied numerically the free convection flows in a square cavity filled with a porous matrix for various boundary conditions and with wide range of parameters, $10^3 \leqslant Ra \leqslant 10^6$, $0.71 \leqslant Pr \leqslant 10$, $10^{-5} \leqslant Da \leqslant 10^{-3}$. Results showed that non-uniform heating of the bottom wall produces greater heat transfer rate at the center of the bottom wall than uniform heating case for all Ra, but average Nu shows overall lower heat transfer rates for non-uniform heating case.

A few studies on natural convection on triangular enclosures filled with a viscous fluid [13] or a porous medium [14,15] have been carried out by earlier researchers. Some of the earlier works [14,15] are based on convection patterns in building attic spaces which are filled with porous material. The scaling analysis and numerical simulations were carried out in these studies and it was found that distinct thermal boundary layers exist if $Ra^{\frac{1}{2}}\frac{H}{L} > 1$, where $\frac{H}{L}$ is the height/length geometric ratio of the attic-shaped porous layer. Although a number of papers deal with heat transfer studies on various applications in triangular porous spaces, a comprehensive analysis on heat transfer and flow circulations is yet to appear in literature.

The aim of the present paper is to provide a complete understanding about the definition of the problem, solution procedure using finite element method and a detailed study of the temperature and flow field with detailed analysis on heat transfer evaluation. The geometry of the triangular enclosure with boundary conditions is shown in Fig. 1. The Darcy–Forchheimer model without the Forchheimer's inertia term has been adopted. The jump discontinuities in Dirichlet type of wall boundary conditions at the corner points due to uniform heating correspond to computational singularities (see Fig. 1). In particular, the singularity at the bottom corner nodes needs special attention. One of the ways for handling the problem is to assume

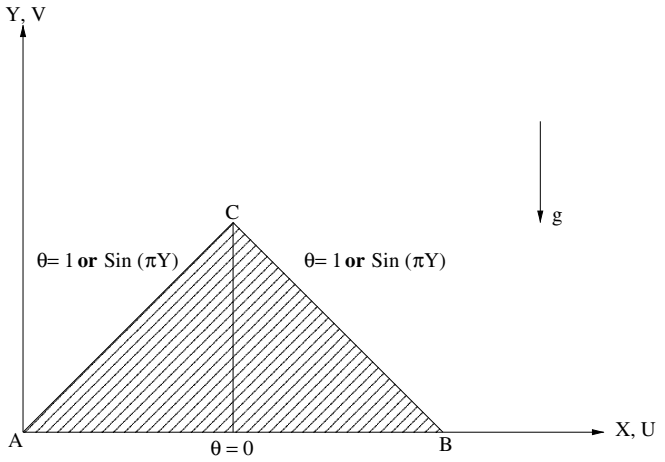

Fig. 1. Schematic diagram of the physical system.

the average temperature of the two walls at the corner as suggested by the earlier works on square cavity [16,12].

In the current study, we have used Galerkin finite element method with penalty parameter to solve the nonlinear coupled partial differential equations governing flow and temperature fields for both uniform and non-uniform temperature distributions prescribed at the side walls. Non-orthogonal grid generation has been done with iso-parametric mapping [17,18]. The grid generation has been done using iso-parametric mapping. Numerical results are obtained to display the circulations and temperature distributions within the triangle and the heat transfer rate for the walls in terms of local and average Nusselt numbers.

2. Governing equations

The physical domain is shown in Fig. 1. Thermophysical properties of the fluid in the flow field are assumed to be constant except the density variations causing a body force term in the momentum equation. The Boussinesq approximation is invoked for the fluid properties with the variation of density with temperature and to couple in this way the temperature field to the flow field. Further, it is assumed that the temperature of the fluid phase is equal to the temperature of the solid phase everywhere in the porous region, and local thermal equilibrium (LTE) is applicable in the present investigation [19]. Also, a velocity square term could be incorporated in the momentum equations to model the inertia effect which is more important for non-Darcy effect on the convective boundary layer flow over the surface of a body embedded in a high porosity media. However, we have neglected this term in the present study because we are dealing with the natural convection flow in a cavity filled with a porous medium. Under these assumptions and following the earlier works [8,20] with the Forchheimer's inertia term neglected, the governing equations for steady two-dimensional natural convection flow in the porous cavity using conservation of mass, momentum and energy can be written with following dimensionless variables

$$X=\frac{x}{L},\quad Y=\frac{y}{L},\quad U=\frac{uL}{\alpha},\quad V=\frac{vL}{\alpha},\quad \theta=\frac{T-T_c}{T_h-T_c}$$
$$P=\frac{pL^2}{\rho\alpha^2},\quad Pr=\frac{\nu}{\alpha},\quad Da=\frac{K}{L^2},\quad Ra=\frac{g\beta(T_h-T_c)L^3Pr}{\nu^2} \tag{1}$$

as:

$$\frac{\partial U}{\partial X}+\frac{\partial V}{\partial Y}=0, \tag{2}$$

$$U\frac{\partial U}{\partial X}+V\frac{\partial U}{\partial Y}=-\frac{\partial P}{\partial X}+Pr\left(\frac{\partial^2 U}{\partial X^2}+\frac{\partial^2 U}{\partial Y^2}\right)-\frac{Pr}{Da}U, \tag{3}$$

$$U\frac{\partial V}{\partial X}+V\frac{\partial V}{\partial Y}=-\frac{\partial P}{\partial Y}+Pr\left(\frac{\partial^2 V}{\partial X^2}+\frac{\partial^2 V}{\partial Y^2}\right)-\frac{Pr}{Da}V+RaPr\theta, \tag{4}$$

$$U\frac{\partial \theta}{\partial X}+V\frac{\partial \theta}{\partial Y}=\frac{\partial^2\theta}{\partial X^2}+\frac{\partial^2\theta}{\partial Y^2}. \tag{5}$$

The boundary conditions are

$$\begin{aligned}&U(X,0)=0=V(X,0),\quad \theta(X,0)=0\quad \text{on AB},\ \forall 0\leqslant X\leqslant 2,\\ &U(X,Y)=0=V(X,Y),\quad \theta(X,Y)=1\\ &\quad \text{or}\quad \sin(\pi Y)\quad \text{on AC},\ Y=X,\ \forall 0\leqslant X\leqslant 1,\\ &U(X,Y)=0=V(X,Y),\quad \theta(X,Y)=1\\ &\quad \text{or}\quad \sin(\pi Y)\quad \text{on BC},\ Y=2-X,\ \forall 1\leqslant X\leqslant 2.\end{aligned} \tag{6}$$

3. Solution procedure

The momentum and energy balance equations (3)–(5) are solved using the Galerkin finite element method. The continuity Eq. (2) will be used as a constraint due to mass conservation and this constraint may be used to obtain the pressure distribution. In order to solve Eqs. (3)–(4), we use the penalty finite element method where the pressure P is eliminated by a penalty parameter γ and the incompressibility criteria given by Eq. (2) which results in

$$P=-\gamma\left(\frac{\partial U}{\partial X}+\frac{\partial V}{\partial Y}\right). \tag{7}$$

The continuity equation [Eq. (2)] is automatically satisfied for large values of γ. Typical values of γ that yield consistent solutions are 10^7. Using Eq. (7), the momentum balance equations [Eqs. (3) and (4)] reduce to

$$U\frac{\partial U}{\partial X}+V\frac{\partial U}{\partial Y}=\gamma\frac{\partial}{\partial X}\left(\frac{\partial U}{\partial X}+\frac{\partial V}{\partial Y}\right)+Pr\left(\frac{\partial^2 U}{\partial X^2}+\frac{\partial^2 U}{\partial Y^2}\right)-\frac{Pr}{Da}U, \tag{8}$$

and

$$U\frac{\partial V}{\partial X}+V\frac{\partial V}{\partial Y}=\gamma\frac{\partial}{\partial Y}\left(\frac{\partial U}{\partial X}+\frac{\partial V}{\partial Y}\right)+Pr\left(\frac{\partial^2 V}{\partial X^2}+\frac{\partial^2 V}{\partial Y^2}\right)-\frac{Pr}{Da}V+RaPr\theta. \tag{9}$$

The system of Eqs. (5), (8), and (9) with boundary conditions (6) are solved by using Galerkin finite element method [17]. The detailed description of the solution procedure is explained in an earlier work [12]. The numerical solutions are obtained in terms of the velocity components (U,V) and stream function (ψ) using the relationship between the stream function (ψ) and the velocity components [21], where the stream function (ψ) is defined in the usual way as $U=\frac{\partial\psi}{\partial Y}$ and $V=-\frac{\partial\psi}{\partial X}$. The no-slip condition is valid at all boundaries as there is no cross flow, hence $\psi=0$ is used for the boundaries.

The heat transfer coefficient in terms of the local Nusselt number (Nu) is defined by

$$Nu=-\frac{\partial\theta}{\partial n}, \tag{10}$$

where n denotes the normal direction on a plane. The local Nusselt number on a surface contains normal derivative as

shown in Eq. (10) and normal derivatives are calculated using the bi-quadratic basis set in $\xi - \eta$ coordinate system.

The local Nusselt numbers at bottom wall (Nu_b), left wall (Nu_l) and right wall (Nu_r) are defined as

$$Nu_b = -\sum_{i=1}^{9} \theta_i \frac{\partial \Phi_i}{\partial Y} \tag{11}$$

$$Nu_l = \sum_{i=1}^{9} \theta_i \left(-\frac{1}{\sqrt{2}} \frac{\partial \Phi_i}{\partial X} + \frac{1}{\sqrt{2}} \frac{\partial \Phi_i}{\partial Y} \right). \tag{12}$$

and

$$Nu_r = \sum_{i=1}^{9} \theta_i \left(\frac{1}{\sqrt{2}} \frac{\partial \Phi_i}{\partial X} + \frac{1}{\sqrt{2}} \frac{\partial \Phi_i}{\partial Y} \right). \tag{13}$$

The average Nusselt numbers at the bottom and side walls are

$$\overline{Nu_b} = \frac{\int_0^2 Nu_b \, dX}{X|_0^2} = \frac{1}{2} \int_0^2 Nu_b \, dX \tag{14}$$

and

$$\overline{Nu_l} = \overline{Nu_r} = \frac{1}{\sqrt{2}} \int_0^{\sqrt{2}} Nu_l \, dS \tag{15}$$

Here dS denotes the elemental length along inclined sides of the triangular cavity as seen in Fig. 1.

4. Results and discussion

4.1. Numerical tests

The computational domain in $\xi - \eta$ coordinates consists of 20×20 bi-quadratic elements which correspond to 41×41 grid points. Note that, the computational grid in the triangular domain is generated via mapping the triangular domain into square domain in $\xi - \eta$ coordinate system [17]. The bi-quadratic elements with lesser number of nodes smoothly capture the non-linear variations of the field variables which are in contrast with finite difference/finite volume solutions available in the literature [6,11]. In addition, we have carried out the validation of the thermal equilibrium for the first time via computing the average Nusselt number for bottom wall which is $\sqrt{2}$ times of that inclined wall as discussed later.

In the current investigation, Gaussian quadrature based finite element method provides the smooth solutions at the interior domain including the corner regions as evaluation of residuals depends on interior gauss points and thus the effect of corner nodes are less pronounced in the final solution. The current finite element approach offers special advantage on evaluation of local Nusselt number at the left and right walls as the element basis functions are used to evaluate the heat flux. For the two cases (I and II), the values of Ra, Da and Pr are considered with wide range to analyze the effects on the heat transfer and fluid flow. The comparative study was made for uniform and non-uniform heating of the side walls. For the brevity of the paper only the most important results are presented in the following sections.

4.2. Uniform heating of side walls (Case I)

Figs. 2–6 display the effects of Da ($Da = 10^{-5}$–10^{-3}), Ra ($Ra = 10^3$–10^6) and Pr ($Pr = 0.026$–10) when the side walls are uniformly heated while the bottom wall is maintained at constant cold temperature. The fluid near the inclined portion of the enclosure is hotter than the fluid near to the cold bottom wall and hence the fluid near the inclined walls have lower density than those near the bottom cold wall. Thus, the fluid near the hot inclined walls move upward resulting in two oppositely rotating circulations in the enclosure. Using the definition of stream function, the streamlines with positive values of ψ correspond to anti-clockwise circulation, and those with negative values of ψ correspond to clock-wise circulation. Note that, for steady flow, stream lines are equivalent to the paths followed by the individual particles in the fluid. Results indicate that the fluid circulations and isothermal lines are strongly dependent on Darcy number as can be seen in the Figs. 2–4.

Fig. 2 illustrates the temperature and stream function contours for $Da = 10^{-5}$ and $Ra = 10^6$, and the flow is seen to be very weak as observed from stream function contours. It may be noted that the maximum value of stream function is 0.15. The temperature contours are smooth and monotonic and this illustrates that heat transfer is

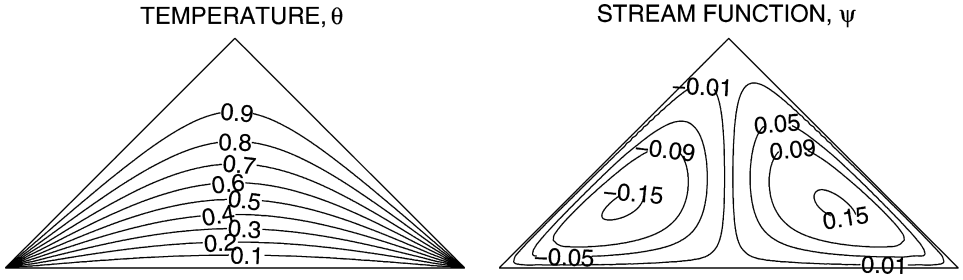

Fig. 2. Temperature and stream function contours for cold bottom wall, $\theta(X,0) = 0$ and uniformly heated inclined walls, $\theta(X,Y) = 1$, with $Da = 10^{-5}$, $Ra = 10^6$ and $Pr = 0.7$ (Case-I). Clockwise and anti-clockwise flows are shown with negative and positive signs of stream function, respectively.

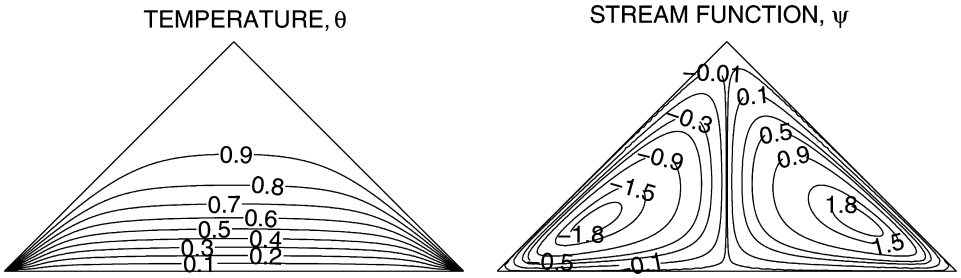

Fig. 3. Temperature and stream function contours for cold bottom wall, $\theta(X,0)=0$ and uniformly heated inclined walls, $\theta(X,Y)=1$, with $Da=10^{-3}$, $Ra=4\times10^{5}$ and $Pr=0.7$ (Case-I). Clockwise and anti-clockwise flows are shown with negative and positive signs of stream function, respectively.

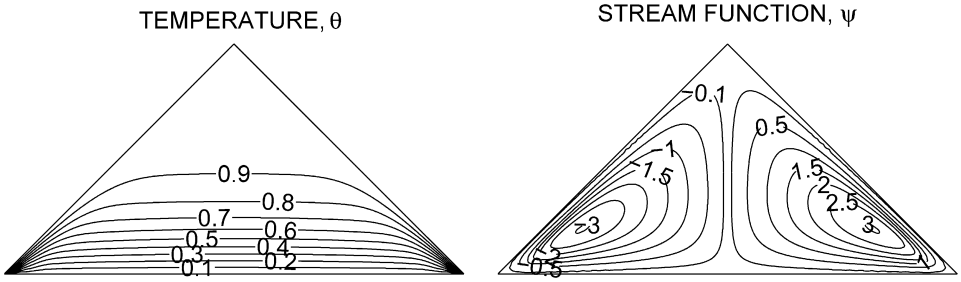

Fig. 4. Temperature and stream function contours for cold bottom wall, $\theta(X,0)=0$ and uniformly heated inclined walls, $\theta(X,Y)=1$, with $Da=10^{-3}$, $Ra=10^{6}$ and $Pr=0.7$ (Case-I). Clockwise and anti-clockwise flows are shown with negative and positive signs of stream function, respectively.

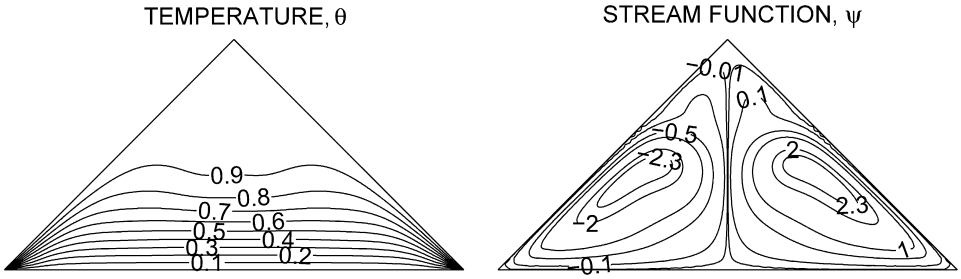

Fig. 5. Temperature and stream function contours for cold bottom wall, $\theta(X,0)=0$ and uniformly heated inclined walls, $\theta(X,Y)=1$, with $Da=10^{-3}$, $Ra=10^{6}$ and $Pr=0.026$ (Case-I). Clockwise and anti-clockwise flows are shown with negative and positive signs of stream function, respectively.

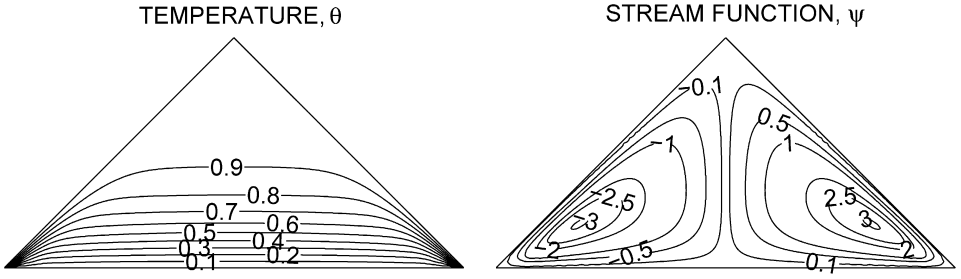

Fig. 6. Temperature and stream function contours for cold bottom wall, $\theta(X,0)=0$ and uniformly heated inclined walls, $\theta(X,Y)=1$, with $Da=10^{-3}$, $Ra=10^{6}$ and $Pr=10$ (Case-I). Clockwise and anti-clockwise flows are shown with negative and positive signs of stream function, respectively.

purely due to conduction. As Da increases to 10^{-3}, the strength of the circulation increases as seen later. The critical Rayleigh number for the conduction dominant mode is found as $Ra=4\times10^{5}$ for $Da=10^{-3}$ and $Pr=0.7$. It may be noted that conduction is dominant below the critical Ra. The value of critical Ra may be obtained from asymptotes of average Nusselt number vs Rayleigh number plot as discussed later. The temperature and stream function plots for critical Ra is shown in Fig. 3. It is observed that at critical Ra the middle portion of the isotherm contours starts getting deformed, and the maximum value of $\psi=1.8$ is at the eye of vortices. As Ra increases to 10^{6}, the buoyancy driven

circulation inside the cavity is also increased as seen from greater magnitudes of the stream function (Fig. 4). The circulations are greater near corner points due to the eye of vortices where maximum value of $\psi = 3$ and least at the wall and at the center due to no slip boundary conditions and no cross flow, respectively. It is observed that the greater circulation in bottom regime follows a progressive wrapping and hence the isotherms are more compressed towards the bottom wall as can be seen in Fig. 4. It is also interesting to note that, the regime near the top corner has no significant thermal gradient resulting in no circulations. Due to high circulations, the temperature contours with $\theta \leqslant 0.7$ are condensed in a very small regime near the bottom wall and consequently, the temperature gradients near the bottom wall are found to be significantly high. It is observed that 80% of the isotherms are confined to only 30% of the triangle near the bottom wall.

Comparative studies on Figs. 5 and 6 show that as Pr increases from 0.026 to 10, the values of stream function and isotherms in the core cavity increase. The similar qualitative features of stream function and isotherms are also found for $Pr = 10$ and $Pr = 1000$ (figures not shown). It is interesting to note that, the greater circulations due to higher Pr leads to elliptical stream function deformed towards the corner points. At high Pr, the stream functions except near the eyes of vortices are almost triangular indicating higher intensity of flows. The temperature and flow behaviors for a representative high Pr ($Pr = 10$) are shown in Fig. 6.

4.3. Non-uniform heating of side walls (Case II)

Figs. 7 and 8 illustrate the stream function and isotherm contours when the inclined walls are non-uniformly heated via sinusoidal function. As seen in Figs. 2–6, uniform heating of inclined walls causes a finite discontinuity in Dirichlet type of boundary conditions for the temperature distribution at both edges of the bottom wall. In contrast, the non-uniform heating removes the singularity at the edges of bottom wall and provides a smooth temperature distribution in the entire enclosure. For $Da = 10^{-5}$–10^{-3}, the circulation pattern is qualitatively similar to the uniform heating case for larger values of Pr ($Pr \geqslant 0.7$). However, compared to uniform heating case, the temperature contours are more compressed near the side walls of enclosure. At $Ra = 10^6$ and $Pr = 0.026$, the isotherms with $\theta \leqslant 0.6$ are pushed towards the bottom wall and consequently the temperature gradients near the bottom wall are significant (Fig. 7). This is due to the fact that the strong primary circulations occur near the center (Fig. 7). In addition, the secondary circulations also occur near the center of the bottom wall which caused the eyes of primary vortices to shift at the center. Further the eyes of primary vortices at the center push the isotherms near the side walls and at the vertex. It is also interesting to note that, the circulations are stronger than uniform heating case (see Fig. 5) and the maximum value of $\psi = 3.8$ is found. It may be noted that, the conduction dominant heat transfer is observed upto $Ra = 4 \times 10^5$.

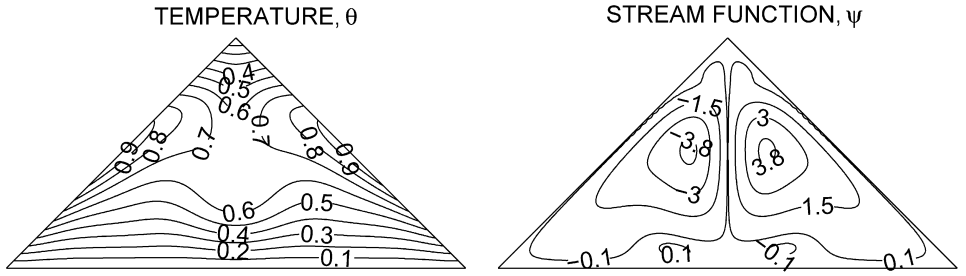

Fig. 7. Temperature and stream function contours for cold bottom wall, $\theta(X,0) = 0$ and non-uniformly heated inclined walls, $\theta(X,Y) = \sin(\pi Y)$, with $Da = 10^{-3}$, $Ra = 10^6$ and $Pr = 0.026$ (Case-II). Clockwise and anti-clockwise flows are shown with negative and positive signs of stream function, respectively.

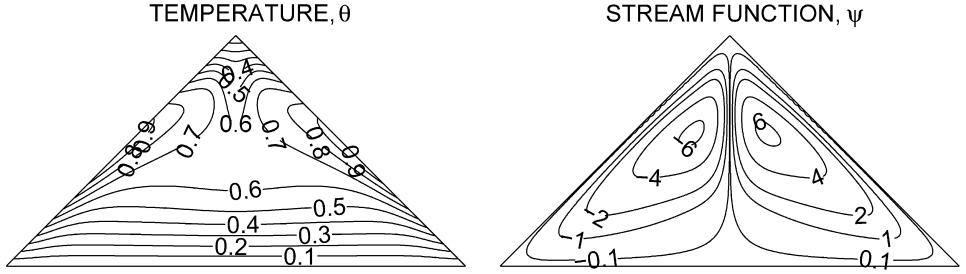

Fig. 8. Temperature and stream function contours for cold bottom wall, $\theta(X,0) = 0$ and non-uniformly heated inclined walls, $\theta(X,Y) = \sin(\pi Y)$, with $Da = 10^{-3}$, $Ra = 10^6$ and $Pr = 0.7$ (Case-II). Clockwise and anti-clockwise flows are shown with negative and positive signs of stream function, respectively.

At $Pr = 0.7$, the isotherms with $\theta \leqslant 0.5$ further pushed towards the bottom wall as seen in Fig. 8. In addition, the greater circulations near the top corner or the eyes of vortices near the top corner push the isotherms within a very narrow regime at the vertex and that results in large thermal gradient at top corner point. In contrast, the circulations near the bottom corner point is large for uniform heating and large thermal gradient occurs near the bottom wall. The flow intensity is found to be enhanced with Pr and it is observed that maximum value of stream function is 3.8 with $Pr = 0.026$ whereas maxima is 6 for $Pr = 0.7$ (Figs. 7 and 8). Due to non-uniform heating of inclined walls, the heating rate near to bottom corners of the inclined walls is generally lower. Results indicate that the strength of the circulations is more for non-uniform heating case than uniform heating.

4.4. Heat transfer rates: local Nusselt numbers

Fig. 9a and b displays the effects of Da ($Da = 10^{-5}$–10^{-3}) and Pr ($Pr = 0.7, 10$) on the local Nusselt numbers at the cold bottom wall and hot inclined walls corresponding to a high Rayleigh number ($Ra = 10^6$). In case of uniform heating of the bottom wall (see Fig. 9a), due to presence of discontinuity in the temperature boundary condition at the edges of bottom wall, the heat transfer rate is very high at these corners and this is common to all Darcy number and Prandtl numbers. Moreover it reduces towards the middle of the bottom wall as the temperature contours are well dispersed at the middle for $Da = 10^{-5}$. The central regime of the bottom wall ($X = 1$) corresponds to larger Nu for $Da = 10^{-3}$ as the compression of the isotherms is significant near the central regime of the bottom wall. At the inclined wall (see Fig. 9b), heat transfer rate is maximum at the bottom edge and minimum at the top edge for all Darcy numbers. As Da increases from 10^{-5} to 10^{-3}, isotherm lines are pushed towards the bottom wall from the inclined walls. Therefore, at the junction of bottom wall, the thermal gradients are relatively more and therefore the heat transfer rate is maximum at the bottom edge of the inclined wall. It is interesting to note that the local Nusselt number tends to zero near the vertex due to uniform temperature distribution.

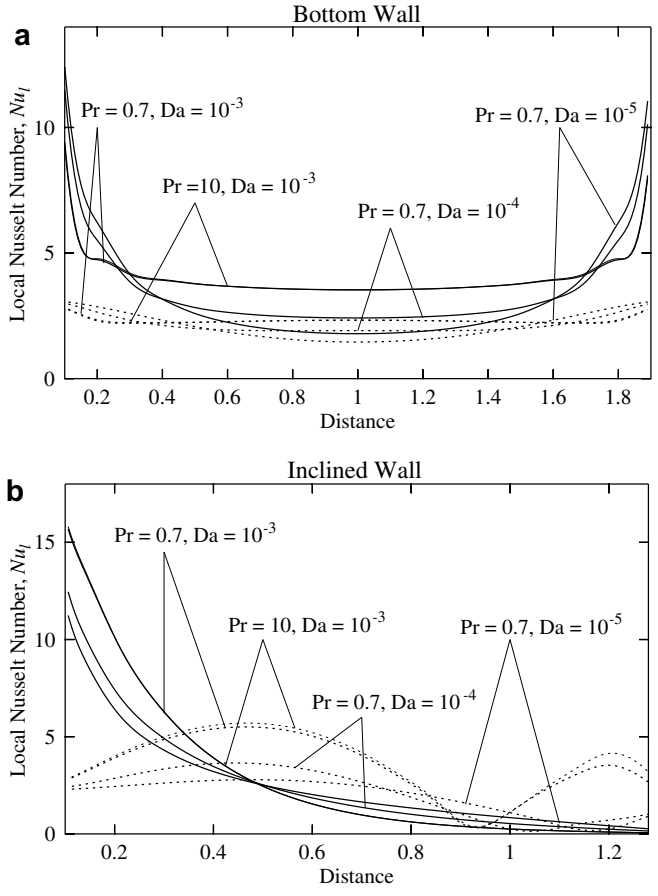

Fig. 9. Variation of local Nusselt number with distance for $Pr = 0.7$ and 10 with $Ra = 10^6$ at: (a) bottom wall (b) inclined wall for uniformly (—) and non-uniformly (---) heated inclined walls and cold isothermal bottom wall.

In the case of non-uniform heating (see Fig. 9a), the local Nusselt number is almost constant for $Da = 10^{-4}$ throughout the bottom wall due to conduction dominant mode of heat transfer. As Da increases from 10^{-5} to 10^{-3}, there is a maximum value of thermal gradient at $X = 1$ due to increased primary circulation and that results in maximum local heat transfer rate (Nu) at $X = 1$. It is interesting to observe that, the non-uniform heating strategy produces a sinusoidal type of local heat transfer rate with its maximum value at the center and edges of bottom wall. At the inclined wall (see Fig. 9b), the local Nusselt number curve for $Da = 10^{-5}$ shows monotonic decrease from bottom edge to a certain region near to top edge of the inclined wall and local Nu has a maximum value at the top edge of the inclined wall due to the compression of isotherms near the vertex. Note that, the local Nusselt number have more wavy distributions for Prandtl number ($Pr = 0.7, 10$) as seen in Fig. 9b due to stronger primary circulations in presence of non-uniform heating. At $Da = 10^{-3}$, there are two local maxima of Nusselt number for the inclined wall as the isotherms are compressed near the top corner and the central regime of inclined wall.

4.5. Overall heat transfer rate and average Nusselt numbers

The overall effects upon the heat transfer rates are displayed in Fig. 10 where the distributions of the average Nusselt number of the bottom and inclined walls, respectively, are plotted vs the logarithmic Rayleigh number. As a verification of the thermal equilibrium of the present steady state system, numerical values of the average Nusselt numbers on bottom and inclined walls are compared and it is found that the average Nusselt number of bottom wall is nearly $\sqrt{2}$ times of average Nusselt number of side wall as the length of the side wall is $\sqrt{2}$. Fig. 10 is shown for Da varying within 10^{-5}–10^{-3} and $Pr = 0.7$. It is interesting to note that the average Nusselt number increases

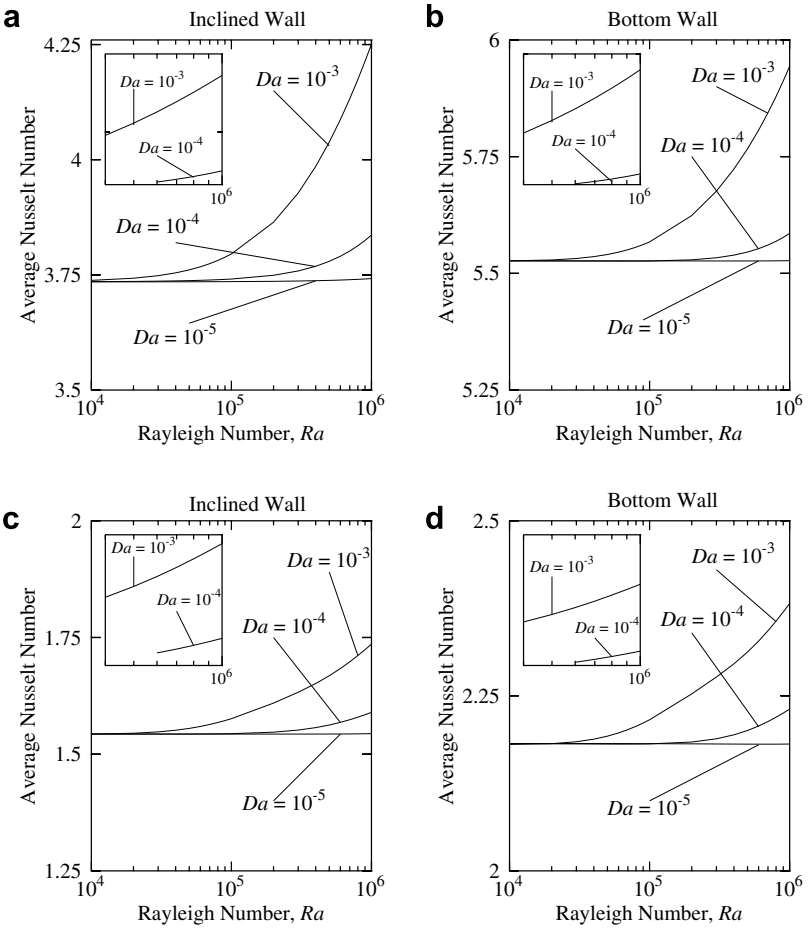

Fig. 10. Variation of average Nusselt number with Rayleigh number for uniformly heated [(a) and (b)] and non-uniformly heated inclined walls [(c) and (d)] for $Da = 10^{-5}$–10^{-3} with $Pr = 0.7$. The insets show the log–log plot of average Nusselt number vs. Rayleigh number for convection dominant regimes.

significantly with Darcy number in the case of uniform heating. It may be remarked that the overall heat transfer rate (average Nusselt number) is less in non-uniform heating as compared to uniform heating due to the less heat input to the system for all Darcy number regimes. For the uniform heating case, it is observed that average Nusselt numbers for both the bottom and inclined walls remain constant for $Da = 10^{-5}$ during the entire Rayleigh number regime. This illustrates the conduction dominant heat transfer for low Darcy number regime irrespective of Rayleigh numbers. As Da increases, the conduction dominant heat transfer regime is narrowed down (see Fig. 10a and b). For conduction dominant heat transfer, the average Nusselt number is in general constant irrespective of Ra.

For non-uniform heating case, it is also interesting to observe that the average Nusselt number for both the bottom and inclined walls is almost constant irrespective of Ra for $Da = 10^{-5}$ (see Fig. 10c and d). This is due to the fact that the flow circulations may cause the isotherm contours to be widely dispersed near the bottom and inclined walls. However, at higher Da, the circulations still cause large temperature gradient near the bottom and inclined walls for higher Ra and hence the increase in average Nusselt number with Darcy number is monotonic. Similar situation is also observed for $Pr = 10$ (figure not shown to brief the manuscript).

The insets show the log-log plot for average Nusselt number vs Rayleigh number for convection dominant regimes. The following correlations with Prandtl number $Pr = 0.7$ are obtained for case I (uniform heating) and case II (non-uniform heating) as follows:

Case I: uniform heating of inclined walls

$$\begin{aligned}\overline{Nu_b} &= \sqrt{2}\overline{Nu_s} \\ &= 4.7652Ra^{0.0115}, \quad Ra \geqslant 6.0\times10^5; \quad Da = 10^{-4} \\ &= 3.3564Ra^{0.0413}, \quad Ra \geqslant 4.0\times10^5; \quad Da = 10^{-3}\end{aligned} \tag{16}$$

Case II: non-uniform heating of inclined walls

$$\begin{aligned}\overline{Nu_b} &= \sqrt{2}\overline{Nu_s} \\ &= 1.6618Ra^{0.0213}, \quad Ra \geqslant 6.0\times10^5; \quad Da = 10^{-4} \\ &= 1.3617Ra^{0.0404}, \quad Ra \geqslant 4.0\times10^5; \quad Da = 10^{-3}\end{aligned} \tag{17}$$

5. Conclusions

The prime objective of the current investigation is to analyze the temperature and flow field with detailed analysis on heat transfer evaluation for natural convection in triangular enclosure filled with porous matrix. The momentum transfer in the porous region is modeled by using Darcy–Forchheimer law. The penalty finite element method helps to obtain smooth solutions in terms of stream function and isotherm contours for wide ranges of Da ($Da = 10^{-5}$–10^{-3}), Ra ($Ra = 10^3$–10^6) and Pr ($Pr = 0.026$–10) with uniform and non-uniform heating of side walls. Results indicate that at low Darcy number ($Da = 10^{-5}$), the isotherm lines are smooth and monotonic for all the Ra and Pr considered. The magnitudes of the stream function contours are very low. This illustrates that at low Da the flow is mostly due to conduction. As Da increases ($Da = 10^{-3}$), the intensity of circulation increases. Consequently, the isotherms are distorted and they are found to be confined within some small regimes near the bottom wall of the triangle.

The conduction dominant heat transfer mode is observed for $Ra \leqslant 4 \times 10^5$ especially for $Da = 10^{-3}$ during uniform and non-uniform heating of the side walls. At the onset of convection dominant mode, the temperature contour lines get compressed towards the bottom wall and the compression is more for uniform heating. It is also interesting to observe that, the temperature contours are more compressed near the central regime or top corner of the inclined wall for non-uniform heating of inclined walls. The effect of Prandtl number is studied to analyze the flow behavior and heat transfer rates for $Da = 10^{-3}$ with $Ra = 10^6$. The shapes of the stream function contours are circular in nature at $Pr = 0.026$ and the shapes would follow the triangular/elliptical structure at high Pr ($Pr = 10$). It may be inferred that at low Prandtl numbers geometry does not have much influence on flow structure. At high Prandtl numbers, geometry has considerable effect and hence the stream function contours are nearly triangular in shape. It is also observed that, as Pr increases from 0.026 to 10, the values of stream function and isotherms in the core cavity increase.

The heat transfer effects are analyzed with local and average Nusselt numbers. It is observed that the local Nusselt numbers for the bottom wall are maximum at the bottom corner points for uniform heating. On the other hand the local Nusselt number shows little variations due to non-uniform heating especially for $Da \leqslant 10^{-4}$. The local Nusselt number distribution shows wavy nature for high Da ($Da = 10^{-3}$) with $Pr = 0.7$ for both uniform and non-uniform heating cases. The local Nusselt number for the inclined walls has two maxima at the center and top region due to the compression of isotherms. The heat transfer rates due to non-uniform heating at these two regimes are higher than uniform heating case. The average Nusselt number illustrates overall lower heat transfer rates for sinusoidal or non-uniform heating cases.

Acknowledgements

Authors wish to express sincere thanks to the reviewer for the valuable suggestions and comments on our paper.

References

[1] A. Bejan, D. Poulikakos, The nondarcy regime for vertical boundary layer natural convection in a porous medium, Int. J. Heat Mass Transfer 27 (1984) 717–722.
[2] D. Poulikakos, A. Bejan, Natural convection in a porous layer heated and cooled along one vertical side, Int. J. Heat Mass Transfer 27 (1984) 1879–1891.
[3] K.R. Blake, A. Bejan, D. Poulikakos, Natural convection near 4 °C in a water saturated porous layer heated from below, Int. J. Heat Mass Transfer 27 (1984) 2355–2364.
[4] D. Poulikakos, A. Bejan, B. Selimos, K.R. Blake, High Rayleigh number convection in a fluid overlaying a porous bed, Int. J. Heat Fluid Flow 7 (1986) 109–116.
[5] K.L. Walker, G.M. Homsy, Convection in a porous cavity, J. Fluid Mech. 87 (1978) 449–474.
[6] T.W. Tong, E. Subramanian, A boundary layer analysis for natural convection in vertical porous enclosures: use of the Brinkman-extended Darcy model, Int. J. Heat Mass Transfer 28 (1985) 563–571.
[7] G. Lauriat, V. Prasad, Natural convection in a vertical porous cavity: a numerical study for Brinkman-extended Darcy formulation, Trans. ASME J. Heat Transfer 109 (1987) 688–696.
[8] K. Vafai, C.L. Tien, Boundary and inertia effects on flow and heat transfer in porous media, Int. J. Heat Mass Transfer 24 (1981) 195–203.
[9] D. Poulikakos, A. Bejan, The departure from Darcy flow in natural convection in a vertical porous layer, Phys. Fluids 28 (1985) 3477–3484.
[10] D. Poulikakos, A departure from the Darcy model in boundary layer natural convection in a vertical porous layer with uniform heat flux from the side, ASME J. Heat Transfer 107 (1985) 716–720.
[11] G. Lauriat, V. Prasad, Non-Darcian effects on natural convection in a vertical porous enclosure, Int. J. Heat Mass Transfer 32 (1989) 2135–2148.
[12] T. Basak, S. Roy, T. Paul, I. Pop, Natural convection in a square cavity filled with a porous medium: effects of various thermal boundary conditions, Int. J. Heat Mass Transfer 49 (2006) 1430–1441.
[13] Yu. E. Karyakin, Yu. A. Sokovishin, O.G. Martynenko, Transient natural convection in triangular enclosures, Int. J. Heat Mass Transfer 31 (1988) 1759–1766.
[14] A. Bejan, D. Poulikakos, Natural convection in an attic shaped space filled with porous material, J. Heat Transfer-Trans. ASME 104 (1982) 241–247.
[15] D. Poulikakos, A. Bejan, Numerical study of transient high Rayleigh number convection in an attic-shaped porous layer, J. Heat Transfer-Trans. ASME 105 (1983) 476–484.
[16] T. Basak, S. Roy, A.R. Balakrishnan, Effects of thermal boundary conditions on natural convection flows within a square cavity, Int. J. Heat Mass Transfer 49 (2006) 4525–4535.
[17] J.N. Reddy, An Introduction to the Finite Element Method, McGraw-Hill, New York, 1993.
[18] T.J. Chung, Computational Fluid Dynamics, Cambridge University Press, London, 2002.
[19] D.A. Nield, A. Bejan, Convection in Porous Media, Springer-Verlag, New York, 1999.
[20] Z.G. Du, E. Bilgen, Natural convection in vertical cavities with internal heat generating porous medium, Wärme-und Stoffübertr 27 (1992) 149–155.
[21] G.K. Batchelor, An Introduction to Fluid Dynamics, Cambridge University Press (1993).